

Published in IET Electrical Systems in Transportation  
 Received on 2nd July 2010  
 Revised on 18th April 2011  
 doi: 10.1049/iet-est.2010.0048

Selected papers from the Power Electronics, Machines  
 and Drives (PEMD'10) Conference



ISSN 2042-9738

# Integration of a mean-torque diesel engine model into a hardware-in-the-loop shipboard network simulation using lambda tuning

A.J. Roscoe<sup>1</sup> I.M. Elders<sup>1</sup> J.E. Hill<sup>2</sup> G.M. Burt<sup>1</sup>

<sup>1</sup>Institute for Energy and Environment, University of Strathclyde, Glasgow G1 1XW, UK

<sup>2</sup>Rolls-Royce PLC, Derby, UK

E-mail: andrew.roscoe@eee.strath.ac.uk

**Abstract:** This study describes the creation of a hardware-in-the-loop (HIL) environment for use in evaluating network architecture, control concepts and equipment for use within marine electrical systems. The environment allows a scaled hardware network to be connected to a simulation of a multi-megawatt marine diesel prime mover, coupled via a synchronous generator. This allows All-Electric marine scenarios to be investigated without large-scale hardware trials. The method of closing the loop between simulation and hardware is described, with particular reference to the control of the laboratory synchronous machine, which represents the simulated generator(s). The fidelity of the HIL simulation is progressively improved in this study. First, a faster and more powerful field drive is implemented to improve voltage tracking. Second, the phase tracking is improved by using two nested proportional–integral–derivative–acceleration controllers for torque control, tuned using lambda tuning. The HIL environment is tested using a scenario involving a large constant-power load step. This provides a very severe test of the HIL environment, and also reveals the potentially adverse effects of constant-power loads within marine power systems.

## 1 Introduction

Recent years have seen increasing interest in the naval and commercial shipping industries in concepts such as the All-Electric Ship, in which an electric propulsion system is combined with the power network serving other electrical loads. Although these technologies offer significant economic and environmental benefits over traditional architectures, shipbuilders, owners and regulatory authorities must be able to determine that the resulting ships will meet the existing and forthcoming standards of reliability and safety, as well as delivering the promised benefits in maintainability and reduced fuel use.

One approach that has been adopted in meeting this challenge is the construction of a full-scale hardware demonstrator [1]. Although this approach has obvious advantages, it also has several drawbacks, including high costs, limited flexibility and the inability to evaluate equipment at the design stage. Alternatively, evaluation of designs through simulation can be adopted, which removes some of the cost and inflexibility of an all-hardware approach, but requires sufficiently accurate models of all components that are to be included. Where equipment or phenomena are poorly understood or poorly documented, this can be a significant barrier.

A third approach is to adopt a reduced-scale hardware-in-the-loop (HIL) approach [2–6] in which physical machines, drives, cables etc. are used to represent certain parts of the

system, whereas others are represented using simulation models. Key advantages of this approach, which is described in more detail in [7], include the ability to evaluate the actual performance of physical drives, controllers etc., as well as the option to scale the output from large simulated devices such as prime movers in a way, which would not be possible in hardware.

This paper describes the adaption and integration of a model of a large multi-megawatt diesel engine, as developed by the manufacturer, into a kilowatt-scale marine network hardware demonstrator. To improve the fidelity of the HIL experiments, pre-existing laboratory HIL capability described in [7] is augmented; firstly with more powerful field controls, and secondly using a dual-nested control loop using proportional–integral–derivative–acceleration (PIDA) controllers, which are tuned in turn using the ‘lambda-tuning’ approach. In order to demonstrate the effectiveness of the approach, measurements of the HIL network behaviour are compared with equivalent simulations. The test scenario used is a large constant-power load step. It is shown that good agreement between both electrical and mechanical behaviour can be achieved in the HIL simulation.

## 2 Choice of test scenario: constant-power load step

For marine vessels, propeller characteristics are defined from a series of tank tests. Perhaps the most famous, and best

documented, of these are the Wageningen (or Troost) B series. These give the propeller torque as a function of the propeller speed and the axial speed of the propeller through the water [8]. For simplified, quasi-steady-state, calculations, the propeller characteristic (torque as a function of propeller speed) can be approximated as a square law in the first quadrant, that is, the propeller pushing the vessel through the water in the forward direction.

At low vessel speeds, it is usual to control the propeller at a constant speed via a propulsion motor speed-control loop. However, at higher vessel speeds, the response of this type of control scheme is unsatisfactory. Small changes in vessel speed, because of a dynamic change in vessel resistance, lead to large changes in the torque (and electrical power demand) demanded via the propulsion motors. This in turn leads to changes in electrical system frequency, and is particularly problematic at higher sea states. The electrical generators are governed to maintain constant frequency, and therefore the engine fuel demand also fluctuates. Overall, this causes extra stress and wear on the prime movers. Therefore a constant-power propulsion mode is used at higher vessel speeds. Changes in the vessel resistance are then manifested through changes in the vessel speed, which are smoothed through the vessel's inertia, which is usually large.

In modern vessels with an All-Electric design, such constant-power drive systems are relatively easy to implement, using power electronics. However, the impact that a step change in load applied through a constant-power drive can have on a marine power system is large. As an illustration, Figs. 1 and 2 show the resulting generator torque and frequency (speed) from four different load steps of 0.5 pu (per-unit):

1. constant power of 0.5 pu,
2. constant torque of 0.5 pu,
3. torque proportional to electrical frequency,
4. torque proportional to electrical frequency squared.

Clearly, the constant-power load step causes the biggest perturbation to the power system. This is because the torque at the generator shaft is inversely dependent upon engine speed, for a given power, and therefore rises as the

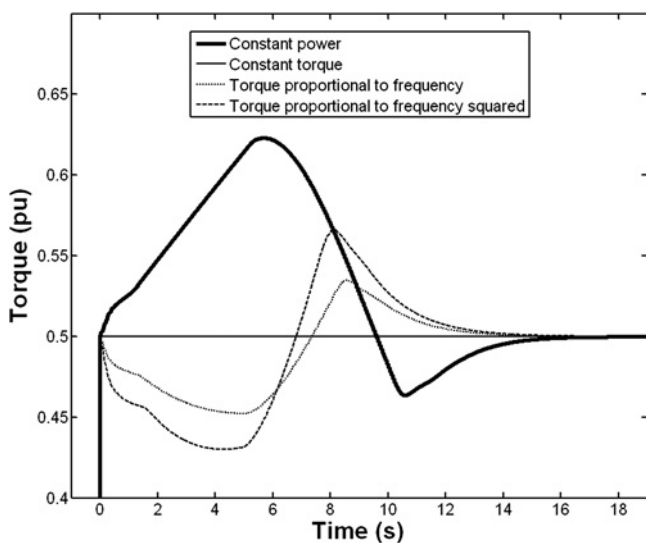


Fig. 1 Generator torque because of 0.5 pu load steps in four different modes

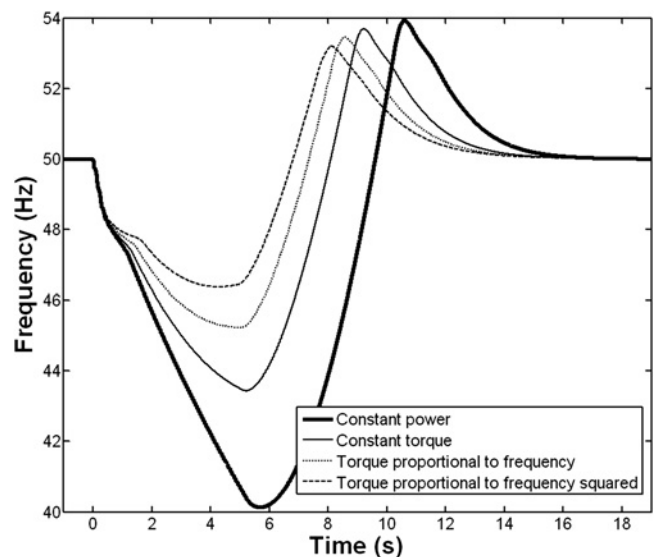


Fig. 2 Generator frequency because of 0.5 pu load steps in four different modes

frequency (engine speed) falls, exacerbating the frequency dip. Sudden introductions of loads in constant torque mode, or where torque falls when speed (frequency) falls, provide much smaller perturbations.

In the following sections, the constant-power load step is studied, since it represents the most interesting and challenging scenario, with rate of change of frequency rates of up to 5 Hz/s. In the scenario, a resistive 0.5 pu load step is applied to an unloaded engine/generator, which is initially at its nominal speed (1 pu, 1500 rpm, giving 50 Hz). The inputs to the engine model are the speed reference (set to an un-drooped value of 1 pu for a 50 Hz target), and the generator torque. The per-unit torque is calculated by the per-unit load power divided by the per-unit frequency. Two cases of this scenario are presented and compared. In the first case ('pure simulation'), the engine model plus the electrical load are simulated. In this case, the electrical load is set to a perfect step function. In the second case, ('HIL'), the engine model is simulated, but the electrical load is applied in hardware using a resistive loadbank. The loadbank is insensitive to frequency, and therefore so long as the system voltage remains at 1 pu, the resistive load behaves as a constant-power load. In both cases, it is assumed that the generator maintains a constant 1 pu voltage during the step, because of effective Automatic Voltage Regulator (AVR) action. In reality, an actual AVR may struggle to maintain nominal voltage during the severe test presented in this study, in the same way that the HIL hardware cannot reduce voltage excursions to exactly zero. However, the assumption of perfect regulation is useful because it provides both the harshest tests of the diesel engine and the HIL hardware, and also it allows simple frequency-insensitive resistive loadbanks to be used in hardware to provide the constant-power load step.

In the hardware (HIL) test, the diesel engine model (which models a machine at the 4 MW scale) was scaled such that its nominal 1 pu power rating was 37.4 kW. Thus, the actual resistive load applied was nominally a resistive 18.7 kW (0.5 pu) at 400 V (1 pu), three-phase, 50 Hz. The scaling to the multi-megawatt model is achieved in this case by simply multiplying the measured electrical power flow in hardware by the factor 4000/37.4, to derive the power (and

hence torque via knowledge of the rotational speed) which would have been extracted from the full-scale diesel.

### 3 Architecture of simulation and HIL implementation

#### 3.1 Simulation of diesel engine

The mean-torque diesel engine model used in this paper is a significant piece of proprietary MATLAB® Simulink® code, supplied by a European manufacturer of marine reciprocating engines. The structure of this simulation model approximately follows that described in [9]. A simpler model, developed specifically for HIL applications, is presented in [10].

The simulation model used in this paper includes a governor controller, the coupling dynamics of the engine to the generator shaft, and also the inertia of, and torque applied to, the generator. The simulation model does not include magnetic phenomena or the electrical behaviour of the generator; the electrical behaviour is determined by the physical synchronous generator.

The diesel model was originally developed in the ‘continuous’ mode within Simulink, and so this has been converted for use with discrete simulations (and HIL applications) by replacing all filters, differentials and integrals with digital equivalents. For this paper, a time step of 2 ms is used, since it matches that used in the HIL application.

#### 3.2 HIL implementation

The diesel engine model can be placed within an HIL environment (Fig. 3). In this case, the aim is to control a real 80 kVA synchronous motor–generator so that it behaves with the same speed/torque and inertial response as the model of the diesel engine and coupled generator. This allows an entire laboratory network of loads, interconnectors, breakers and smaller generators to be connected. The power hardware network can thus be virtually driven by the model of the diesel/generator, and the model of the diesel/generator becomes loaded by the network. The closure of this feedback loop creates an HIL environment. It should be noted that while this paper refers specifically to scenarios where the simulated part consists of a diesel reciprocating engine, the HIL design, functionality and fidelity are applicable to many other types of simulated prime movers, machines or electrical networks. When entire

electrical networks are required to be simulated, an appropriate electrical real-time simulator is required [7].

The 80 kVA motor–generator is driven by a fast responding DC motor coupled to a thyristor drive. The essential details of this implementation are described in [7]. However, in this case the simulation of the diesel engine can be executed on the same computer as the HIL control (the simulator and controller in Fig. 3). Also, the diesel engine model returns a speed output as a response to a torque input, and this speed output must be integrated to provide the phase of  $V_N^*$ . This integration includes an arbitrary (constant) phase offset value, which is essentially a free variable. For these two reasons, so long as the sampled values of  $V_N$ ,  $I_N$  are measured carefully with matched anti-aliasing filters and made coherently (or processed to be coherent as in [7]), then there is essentially zero loop delay. This significantly simplifies the implementation compared to previous work in [7].

### 4 Incremental improvements to HIL fidelity

The 0.5 pu constant-power load step was first applied to the HIL environment using identical field and torque controls for the 80 kVA generator as were originally used in [7]. Specifically, the field control used a rotary exciter and the torque control used a control algorithm shown in Fig. 2 of [7]. It was shown in [7] that although the rotary exciter had sufficient power to maintain steady-state operation, it was lacking in sufficient overhead voltage capability to enable the toughest HIL scenarios to be tracked accurately. This is borne out in the first set of results, shown in Fig. 4, and by the ‘original’ lines in Figs. 11–13. In particular, the poor voltage tracking (Fig. 11) leads to a drop in power flow relative to the pure simulation.

#### 4.1 Improving the accuracy of the voltage tracking at the shared node

To improve the voltage tracking, the rotary exciter for the 80 kVA generator was removed from the HIL hardware, and replaced with a large solid-state DC power supply with a high switching frequency and fast response. This has adequate DC current capability to maintain steady-state terminal voltage at the machine rating. More significantly, it has a much higher available DC voltage than the rotary exciter. This enables the field current to be increased much more rapidly during load changes, allowing terminal voltage to be regulated much better. The particular DC

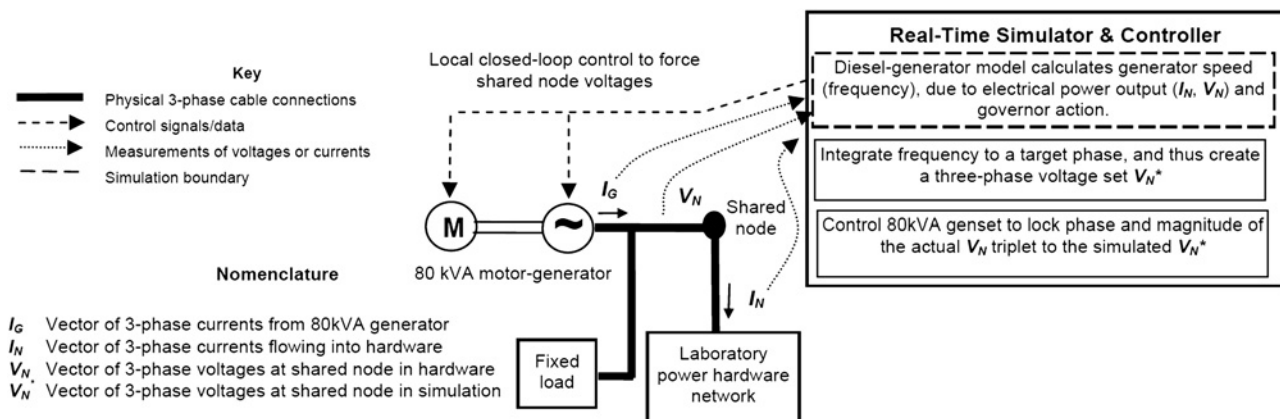
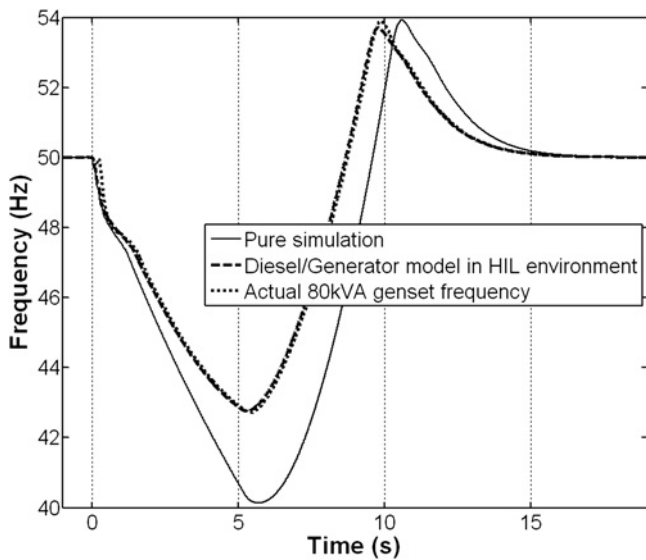


Fig. 3 HIL environment for the diesel/generator model



**Fig. 4** Generator frequency: pure simulation and HIL using original set-up

supply used during this study is only capable of generating positive voltages. For the scenario presented, this is acceptable. For scenarios involving tracking of voltage dips, a bidirectional DC source capable of negative voltage output and reverse power flow would be highly desirable, to allow forcible collapse of the field. The field control contains a proportional–integral–derivative (PID) controller, and the control gains can be increased using the DC supply, owing to the faster response of the field using this hardware.

Using the improved field control leads to the dashed lines in Figs. 11–13. Notably, the voltage tracking error is much reduced, and therefore the power flow in the HIL experiments is much closer to the ‘pure simulation’ case, than with the original set-up.

#### 4.2 Improving the accuracy of the phase tracking at the shared node

In [7], the torque control to the DC motor (driving the 80 kVA generator) was derived using a phase-locking control shown in Fig. 2 of [7]. This consisted of a PID controller to control frequency, using an additional low-pass filter on the

differential control (only) to limit the effects of measurement noise [11], augmented with a simple proportional-only controller to enable tracking of phase. In addition, the values of the control parameters were obtained by hand tuning in the laboratory. The values of these original parameters are shown in Table 1.

To improve the torque control, the ‘lambda-tuning’ approach has been taken, which is a variant of internal model control tuning [12]. To enable this, the parameters for the generator were measured through a series of tests, such as spin-down tests (to measure inertia and friction), and step changes in command torque (to measure drive response). Knowledge of these parameters, combined with knowledge of the measurement algorithms, allows the system to be modelled to the required level of accuracy. The model structure is shown in Fig. 5.

The right-hand loop of Fig. 5 is a conventional loop for controlling frequency to a given target. The left-hand loop augments the control system with the unconventional (but required) control of generator phase to achieve a given target. In the model, this input can be regarded as a zero input for open-loop transfer function (OLTF) stability analysis, or can be used to simulate the effects of measurement noise at different frequencies in a closed-loop transfer function (CLTF) analysis. In order to simplify the control system, the right-hand frequency control loop could be opened during phase control, leaving only the left-hand loop active. However, this means that both the integration (1/s) stages  $H(s)$  – the generator inertia, and  $R(s)$  – the frequency-to-phase transformation, would be present in the OLTF. This means that the phase lag of the OLTF would be  $180^\circ$  even at DC, becoming even more lagged at higher frequencies owing to the action of low-pass filters and measurement times. Stabilising such a loop presents a significant problem requiring large amounts of differential gain. Thus, the control is easier to stabilise if both the control loops are cascaded, since the effect of the inertial lag can be reduced by closing the frequency-control loop.

The round-trip (command to measured value) closed-loop responses for the system, using the original hand-tuned parameters (Table 1), are shown in Fig. 6. The phase loop response represents the entire control system of Fig. 5, whereas the frequency loop response represents the inner frequency-control loop. The phase loop has a bandwidth of about 2 Hz. The OLTF is not shown graphically, but the forecast gain margin is 15.5 dB and the phase margin is  $42^\circ$ .

**Table 1** Control parameters for DC motor torque control

Description	Parameter	Adjustments to (4) and (5)	Final value	Original set-up (hand-tuned)
target frequency CLTF response time	$a$	—	0.15 s	—
target phase CLTF response time	$b$	—	0.02 s	—
frequency loop $C_f$	$K_i$	boosted by $10\times$	3.432	2
frequency loop $C_f$	$K_p$	—	8.935	8
frequency loop $C_f$	$K_d$	—	1.352	1
frequency loop $C_f$	$K_a$	reduced to $1/4\times$	0.008589	—
frequency loop $C_f$ low-pass filter cutoff	$[fa/(f+a)]$	—	66.6 ms	3.18 ms
			2.39 Hz	50 Hz (on $K_d$ control only)
phase loop $C_p$	$K_i$	—	0	—
phase loop $C_p$	$K_p$	—	22.29	$360 \times 0.04 = 14.4$
phase loop $C_p$	$K_d$	—	3.898	—
phase loop $C_p$	$K_a$	reduced to $1/4\times$	0.02078	—
phase loop $C_p$ low-pass filter cutoff	$[pb/(p+b)]$	—	11.1 ms	—
			14.3 Hz	



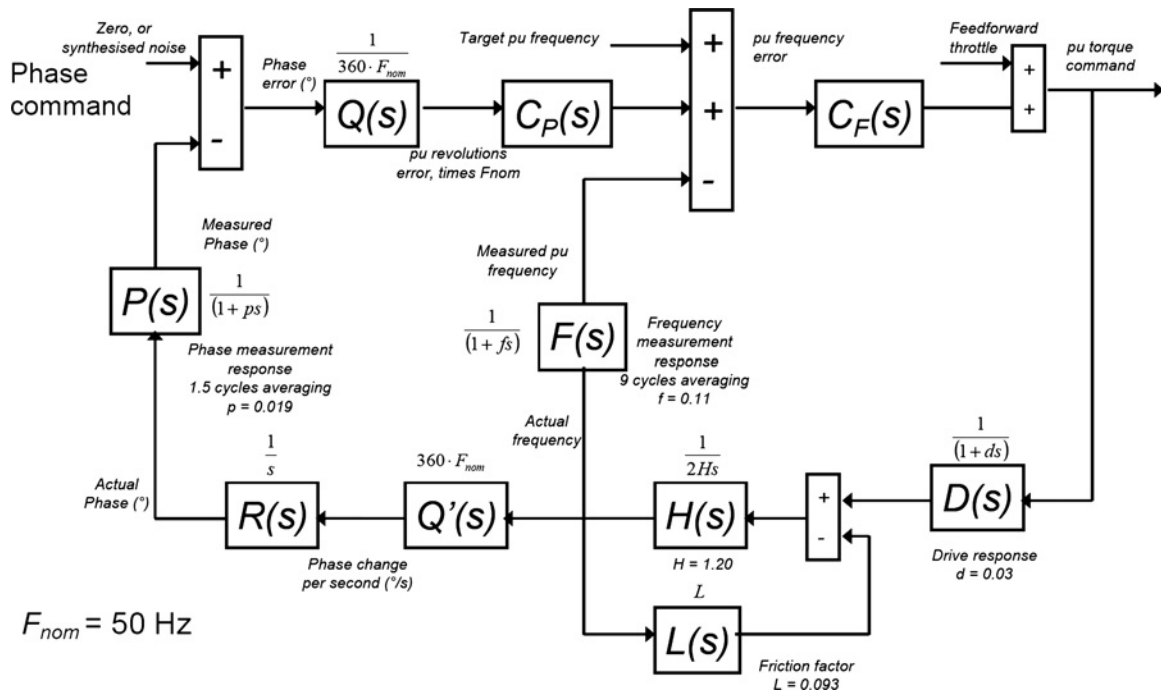


Fig. 5 Torque control system

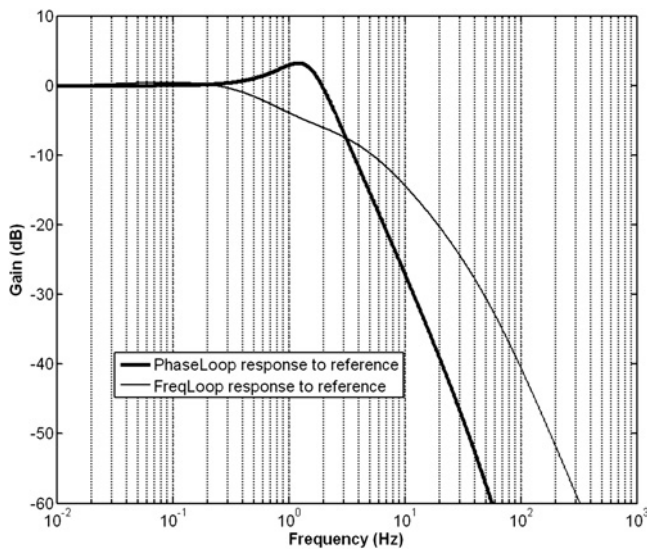


Fig. 6 Command to measured value response of the phase loop and frequency loop: hand-tuned parameters

To improve the response, ‘lambda tuning’ was used [12]. Targets were set for the desired closed-loop command to measured value responses of the frequency-control loop, and then the phase-control loop. The targets are defined such that the responses should ideally behave as first-order low-pass filter responses to command signals. First, the CLTF for the frequency-control loop

$$\frac{(C_F D(H/(1 + HL)))}{(1 + C_F D(H/(1 + HL))F)} = \frac{1}{(1 + as)} \quad (1)$$

where  $a$  is the target first-order response time. Second, the response for the phase-control loop (see (2))

where  $b$  is the target first-order response time.

Assuming that (1) can be satisfied, then (2) can be simplified to

$$\frac{(C_P[\{1/(1 + as)\}]R)}{(1 + C_P[\{1/(1 + as)\}]RP)} = \frac{1}{(1 + bs)} \quad (3)$$

Equations (1) and (3) can be solved, yielding

$$C_F = \frac{[L(1/s) + (2H + L(f + d))] + (2H(f + d) + Lfd)s + 2Hfd s^2}{(f + a)(1 + (fa/(f + a))s)} \quad (4)$$

and

$$C_P = \frac{[0(1/s) + 1 + (a + p)s + ap s^2]}{(p + b)(1 + (pb/(p + b))s)} \quad (5)$$

Equations (4) and (5) define the parameters for the two controllers  $C_F$  and  $C_P$ . Notably, these controllers are unconventional PIDA controllers, combined with low-pass filter elements. The acceleration terms (in  $s^2$ ) dramatically aid the stability, since they counter the phase lags. However, the risk in a practical system is that they (and indeed even the differential controls) introduce large amounts of noise because of the differentiation stages. It is only possible to use these terms, even with reduced magnitude, owing to the good noise reduction of the measurement algorithms [13]

Setting the actual controls in practice involved the following steps, recognising that Fig. 5 is only an estimation of the actual system, and that the simple targets

$$\frac{(QC_P[\{C_F D(H/(1 + HL))\}]/\{1 + C_F D(H/(1 + HL))F\}]Q'R)}{(1 + QC_P[\{C_F D(H/(1 + HL))\}]/\{1 + C_F D(H/(1 + HL))F\}]Q'RP)} = \frac{1}{(1 + bs)} \quad (2)$$

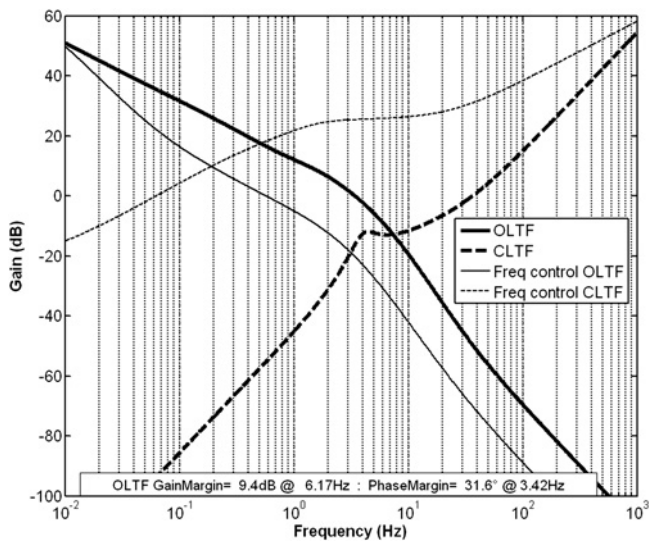


**Fig. 7** OLTF and CLTF bode plots (gain) for lambda-tuned torque control

(1) and (2) do not fully define the response required in all scenarios:

1. choosing response times  $a$  and  $b$ ;
2. evaluating (4) and (5) and then examining OLTF (stability), CLTF (command to output) and response (command to measured value) plots using MATLAB®;
3. trials of the chosen settings in the hardware implementation, making small changes to the settings of  $a$  and  $b$ ;
4. reductions in the actual proportions of acceleration ( $s^2$ ) controls used, from those suggested in (4) and (5), to limit the response to measurement noise, as shown in Table 1;
5. increasing the amount of integral gain in  $C_F$  to improve the initial settling to a new frequency, as shown in Table 1;
6. repetition of trials of steps 2–4, in a range of scenarios, until the best behaviour is achieved.

The final set of control parameters are shown in Table 1, together with the original hand-tuned values.

The resulting bode plots of the OLTF and the command-to-output CLTF are shown in Figs. 7 and 8. Forecast gain margin

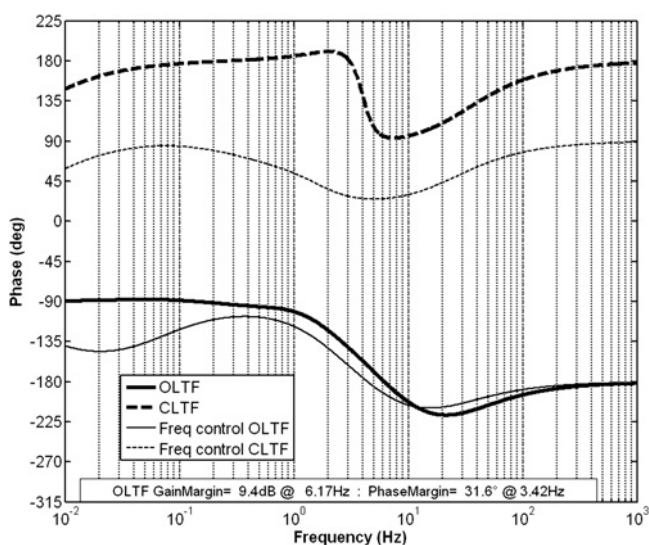


**Fig. 8** OLTF and CLTF bode plots (phase) for lambda-tuned torque control

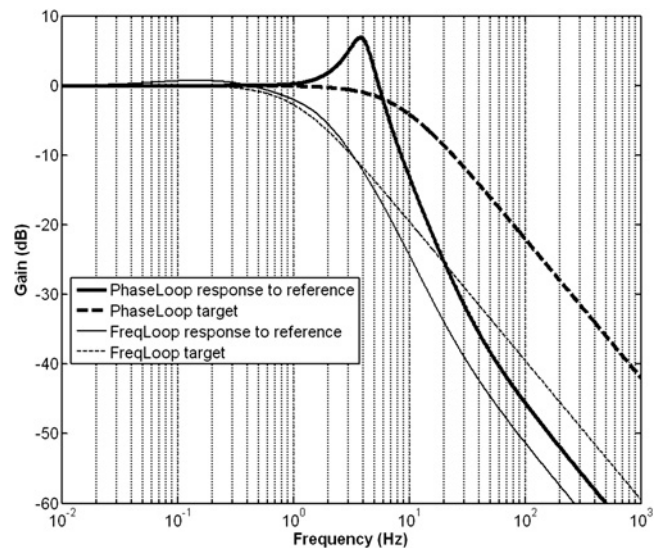


**Fig. 9** Command to measured value response of the phase loop and frequency loop: lambda-tuned parameters

is 9 dB and phase margin is  $32^\circ$ . Indeed, the hardware system is fast responding and on the limit of stability with this configuration. It is certainly found that if the  $Ka$  acceleration terms (in  $s^2$ ) are set to zero, the hardware is unstable. Conversely, if the  $Ka$  terms are increased to their theoretical values, noise becomes intolerable at the torque command output because of the increased CLTF response at high frequencies. The resulting responses (commands to measured values) are shown in Fig. 9. The phase loop bandwidth is increased from about 2 Hz to about 6 Hz. Fig. 9 also shows the predicted deviations from the target ‘lambda-tuned’ response, caused mainly by the one-fourth reductions in the  $Ka$  gains to limit the effects of noise. The  $10\times$  boost to the integral gain of  $C_F$  causes almost no visible change to the responses shown in this figure.

Using the improved controls, the HIL environment is now able to track the ‘pure simulation’ case much more accurately. Fig. 10 shows the frequency profile, with the HIL results now

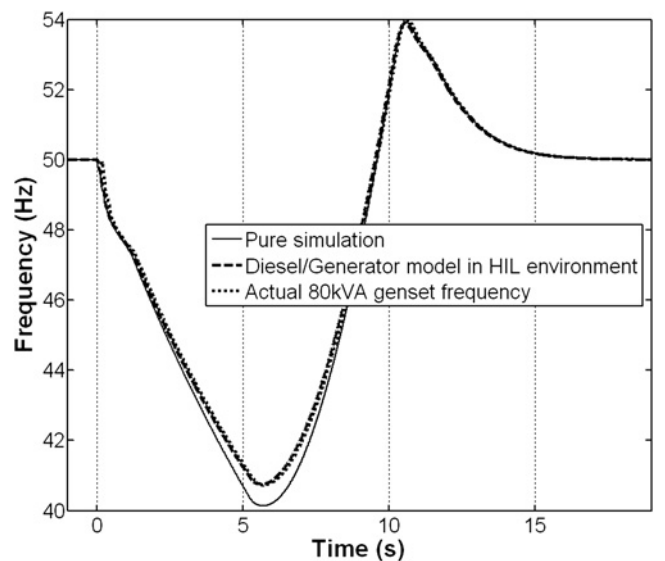


**Fig. 10** Generator frequency: pure simulation and HIL using improved field and torque controls

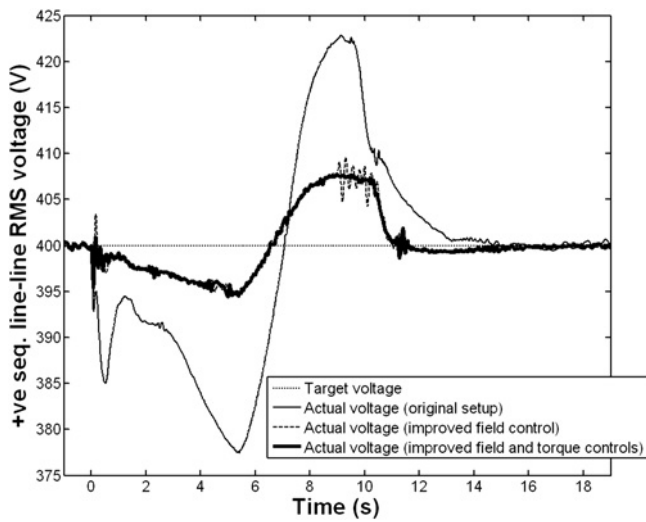


Fig. 11 Voltage tracking for 0.5 pu constant-power step HIL experiments

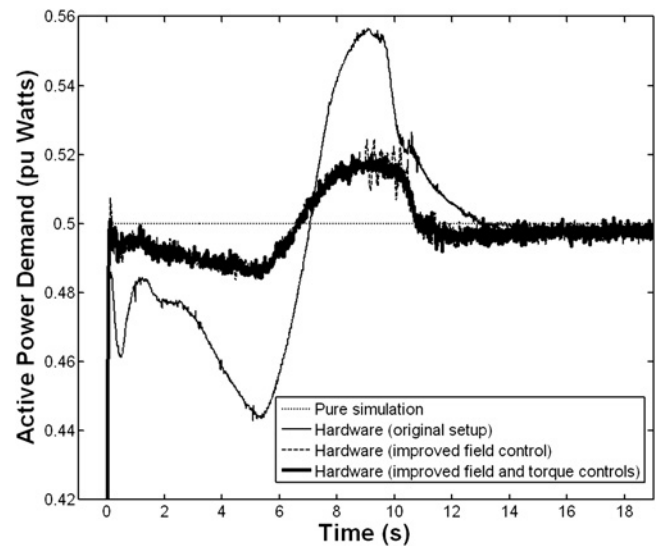


Fig. 13 Power flow for 0.5 pu constant-power step HIL experiments

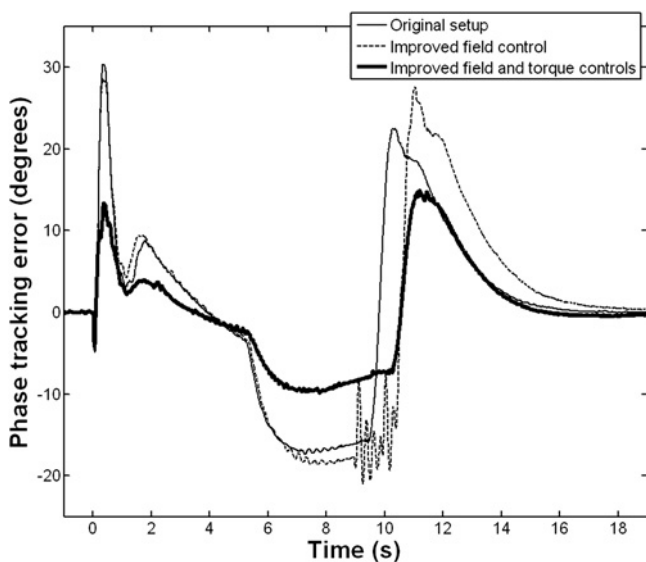


Fig. 12 Phase tracking for 0.5 pu constant-power step HIL experiments

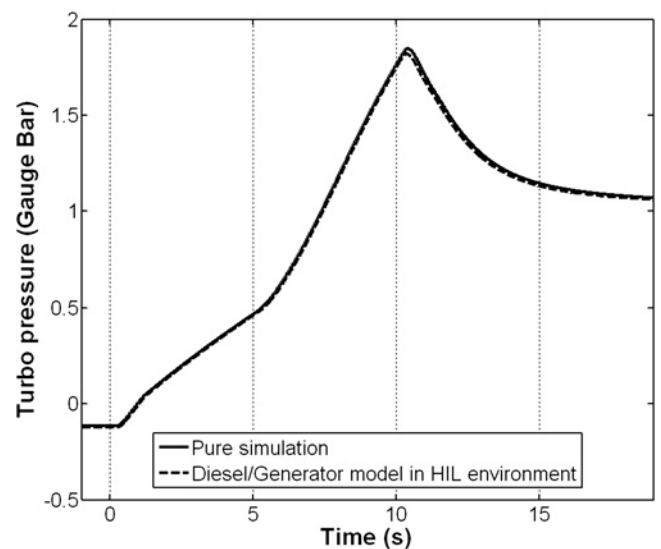


Fig. 14 Turbo pressure

tracking the simulation results much more closely than before (Figs. 10–13). The use of the lambda-tuning approach and the redesign of the torque control allows the peak phase tracking error to be reduced from 30 to 15°.

Of note in the presented scenario is the large frequency dip. This is owing to the behaviour of the turbo charger which takes time to ‘spin up’, especially when engine speed drops in response to the load step. The turbo

pressure (in gauge bar) can be extracted from the HIL model in real time, and is shown in Fig. 14. This shows excellent agreement between the ‘pure simulation’ and the HIL results.

### 4.3 Summary of incremental improvements

The incremental improvements in the fidelity of the HIL environment, from the starting point of the basic controls used in [7], are summarised in Table 2. The incremental

Table 2 Incremental improvement in the fidelity of the 0.5 pu constant-power step HIL experiments

Description	Original set-up as per [7]	Improved voltage tracking (80 kVA field control)	Improved voltage tracking and DC motor control
maximum voltage tracking error, pu	0.058	0.024	0.020
maximum frequency-tracking error, Hz	3.4	0.6	0.6
maximum phase tracking error, deg	30	29	15
maximum power flow tracking error, pu	0.055	0.022	0.018



improvements are first the more powerful and faster-acting field control (Section 4.1), followed by the improved phase tracking using lambda tuning (Section 4.2). The improvements in fidelity are also shown in Figs. 10–13.

## 5 Conclusions

A nested pair of PIDA controllers have been tuned using 'lambda tuning'. These can be used to tightly match the phase of a large synchronous machine to the phase of a simulated machine. This allows a simulation of a multi-megawatt diesel engine to be interfaced with physical hardware to create an HIL simulation environment, suitable for use with marine power system scenarios. The PIDA controllers allow the physical generator to track the phase of the simulated prime-mover to within 10–15° for scenarios with rates of change of frequency up to 5 Hz/s. The phase tracking is much better than this figure for less dynamic scenarios. The phase tracking accuracy cannot be significantly improved from the present performance, owing to the physical limitations of the drive system and machine inertia. However, some further marginal improvements might be made by reducing the measurement algorithm times (Fig. 5). Care would be needed, however, since noise output from these algorithms will degrade the control signals, which make use of unconventional control terms in  $s^2$  to increase the control gain without becoming unstable.

For use within an HIL environment, it is also important that the field control for the synchronous generator be able to rapidly increase or decrease the field current, to track the simulation. This requires a field drive with sufficiently large voltage drive capability. Improved performance was shown in this paper by using a more capable field drive. A bidirectional field drive would also allow scenarios such as sharp voltage dips to be modelled.

Finally, the scenario of a step in constant-power demand is of particular interest in that the resulting torque can be larger than expected if frequency drops appreciably. Since constant-power electrical loads (e.g. solid-state motor drives) are becoming more prevalent, such scenarios are important in any All-Electric Ship design.

## 6 Acknowledgments

The authors would like to acknowledge the funding and support provided by Rolls-Royce PLC, which enabled this work to be undertaken.

## 7 References

- Butcher, M.S., Mattick, D., Cheong, W.J.: 'Informing the AC versus DC debate – the electric ship technology demonstrator'. All Electric Ship (AES), Versailles, France, 2005
- Armstrong, M., Atkinson, D.J., Jack, A.G., Turner, S.: 'Power system emulation using a real time, 145 kW, virtual power system'. European Conf. Power Electronics and Applications, 2005
- Langston, J., Suryanarayanan, S., Steurer, M., Andrus, M., Woodruff, S., Ribeiro, P.F.: 'Experiences with the simulation of a notional all-electric ship integrated power system on a large-scale high-speed electromagnetic transient simulator'. Power Engineering Society General Meeting, 18–22 June 2006
- Liu, Y., Steurer, M., Ribeiro, P.: 'A novel approach to power quality assessment: real time hardware-in-the-loop test bed', *IEEE Trans. Power Deliv.*, 2005, **20**, (2), pp. 1200–1201
- Qian, L., Liu, L., Cartes, D.A.: 'A reconfigurable and flexible experimental footprint for control validation in power electronics and power systems research'. Power Electronics Specialists Conf. (PESC), Orlando, USA, 2007
- Woodruff, S., Boenig, H., Bogdan, F., *et al.*: 'Testing a 5 MW high-temperature superconducting propulsion motor'. Electric Ship Technologies Symp., 25–27 July 2005, pp. 206–213
- Roscoe, A.J., Mackay, A., Burt, G.M., McDonald, J.R.: 'Architecture of a network-in-the-loop environment for characterizing AC power system behavior', *IEEE Trans. Ind. Electron.*, 2010, **57**, (4), pp. 1245–1253
- Hill, J.E., Kinson, A.S., Eraut, N.D., French, C., Tumilty, R.M.: 'Motor load train calculations for a land based Demonstrator for Marine Electrical Networks (DMEN)'. IEE Int. Conf. Power Electronics, Machines and Drives (PEMD), Edinburgh, UK, 2004
- Kao, M.H., Moskwa, J.J.: 'Turbocharged diesel-engine modeling for nonlinear engine control and state estimation', *Trans. ASME, J. Dyn. Syst. Meas. Control*, 1995, **117**, (1), pp. 20–30
- Cooper, A.R., Morrow, D.J., Chambers, K.D.R.: 'A turbocharged diesel generator set model'. Universities' Power Engineering Conf. (UPEC), Glasgow, UK, 2009
- Kristiansson, B., Lennartson, B.: 'Robust tuning of PI and PID controllers – using derivative action despite sensor noise', *IEEE Control Syst. Mag.*, 2006, **26**, (1), pp. 55–69
- Lennartson, B., Kristiansson, B.: 'Evaluation and tuning of robust PID controllers', *IET Control Theory Appl.*, 2009, **3**, (3), pp. 294–302
- Roscoe, A.J., Burt, G.M., McDonald, J.R.: 'Frequency and fundamental signal measurement algorithms for distributed control and protection applications', *IET Gener. Transm. Distrib.*, 2009, **3**, (5), pp. 485–495